Impact of Blade Icing on the Performance of the Kola Wind Power Plant: Modelling and Analysis

I. I. RASTVOROVA[1], V. S. ERMOLOVICH
Department of Electronic Systems,
Saint Petersburg Mining University,
Saint Petersburg,
RUSSIAN FEDERATION

Abstract: - The paper examines the impact of atmospheric icing on wind turbine blades on the energy production of the Kola Wind Power Plant, located in the cold and humid climatic conditions of the Murmansk region. An engineering-oriented numerical model of wind turbine blade icing is developed based on the Makkonen formulation, accounting for meteorological conditions characteristic of the region and the main mechanisms of ice accretion and ablation. The blade is discretized into radial segments, for which ice accumulation and removal processes, residual ice thickness, and the associated degradation of aerodynamic performance and rotor rotational speed are calculated. Based on model simulations, energy production losses for the Kola Wind Power Plant in 2023 are estimated. The results show that during the cold season, atmospheric icing can reduce monthly energy production by approximately 2–15%, depending on the month, while the integral annual losses amount to about 4–5% compared to an ice-free scenario.

Key-Words: - wind turbine, Kola wind farm, icing, numerical modelling, Makkonen model, power losses.

Received: May 21, 2025. Revised: January 6, 2026. Accepted: March 27, 2026. Published: July 7, 2026.

1 Introduction

Wind energy is a key area in the development of renewable energy and plays a crucial role in the transition to a low-carbon economy. Over the past few decades, the installed capacity of wind turbines has increased significantly, and their geographical distribution has expanded due to the deployment in northern and high-latitude regions with high and persistent wind resources. Alongside the obvious advantages, wind power faces a number of operational and climatic challenges. One of the most important factors affecting the efficiency of wind turbines is the stability and predictability of wind flows, [1]. Consequently, wind farms are increasingly being located in regions with high wind speeds and high wind constancy, [2]. Particular interest is attracted by northern and cold regions, where the wind is more stable, and the dense cold air has an increased energy potential, [3]. According to the International Energy Agency (IEA), the total installed capacity of wind power in cold regions increased from 156 GW in 2020 to 224 GW by the end of 2025 [4], which indicates substantial growth in this segment.

For Russia, with its vast Arctic and sub-Arctic territories and numerous remote settlements, wind energy is considered a promising way to reduce dependence on diesel generation and to improve the reliability of power supply, [5], [6].

The operation of wind turbines in cold climates is associated with specific challenges, among which one of the most significant is blade icing. Ice accretion resulting from the interaction of blades with supercooled water droplets and snow leads to changes in the aerodynamic profile, increased surface roughness, and a reduction in rotor power coefficient. According to international studies, annual energy production losses due to icing can reach and exceed 20 %, and in some cases, icing leads to prolonged forced shutdowns of turbines and increased operating costs. Non‑uniform ice mass distribution along the blade causes additional vibration and structural loads, while ice shedding from rotating blades poses safety risks to personnel and nearby infrastructure, [7].

For wind power facilities located in the northern regions of Russia, such as the Kola Peninsula, the icing problem is particularly acute. The Kola wind power plant (Kola WPP) operates under frequent sub‑zero temperatures, high humidity, and complex atmospheric conditions; however, quantitative assessments of the impact of icing on its performance are still limited and are mainly based on generalized statistical approaches, [8].

In this study, an engineering-oriented numerical model of wind turbine blade icing is proposed for the conditions of the Kola wind power plant, based on the Makkonen formulation and using the liquid water content in air as a key parameter diagnosed from air temperature, relative humidity, and present weather type. Ice accretion and ablation, including the possibility of mechanical shedding, are modelled on discrete blade segments and are linked to changes in rotor rotational speed and potential turbine shutdowns through a simplified engineering model of aerodynamic performance degradation. Based on model simulations for the cold period of the year, the impact of icing on turbine operating regimes and potential energy production losses at the Kola wind power plant is assessed.

2 Physical and Meteorological Background for Atmospheric Icing Modelling

2.1 Atmospheric Icing of Wind Turbine Blades

Atmospheric icing of wind turbine blades is caused by the deposition of liquid and solid water phases on the surface of the aerodynamic profile and may occur both as a result of in-cloud processes (fog and low-level clouds containing supercooled droplets) and due to precipitation. Depending on meteorological conditions and the ice formation mechanism, several characteristic types of ice accretion are distinguished, among which the most common are glaze (clear ice), rime (rough ice), and mixed icing.

Glaze icing forms predominantly at air temperatures around 0…–10 °C and high concentrations of supercooled liquid water. It leads to the formation of a dense, strongly bonded ice layer and significantly alters the aerodynamic profile of the blade, [9]. Rime icing is typical of lower temperatures and lower liquid water content; it is characterized by a porous structure and, as a rule, lower density, [10]. Icing associated with wet snow and mixed precipitation occurs in the presence of a liquid water phase within partially melted snow particles and may result in the formation of dense but mechanically unstable ice deposits.

Under real wind turbine operating conditions, mixed icing is frequently observed, when temperature, humidity, and precipitation type vary within a single icing event. Differences between icing types manifest themselves through variations in the efficiency of water capture and accretion, ice density, and adhesion strength to the blade surface. In engineering-oriented icing models, these effects are typically accounted for by means of effective coefficients introduced into the ice mass growth equations, [11].

2.2 Meteorological Factors and Representation of Liquid Water Content (LWC)

The intensity of atmospheric icing is governed by a combination of several meteorological factors, including air temperature, relative humidity, wind speed, and the presence of supercooled liquid water. The most unfavorable conditions generally occur at air temperatures in the range of approximately –2…–10 °C and relative humidity exceeding 85–90 %, particularly in the presence of fog or low-level clouds containing supercooled droplets, [12]. An increase in mean wind speed enhances impingement icing due to higher relative collision velocities between hydrometeors and the blade surface and leads to a wider radial extent of icing along the blade span. The type of precipitation and present weather phenomena (fog, freezing rain, drizzle, snow, ice pellets) determine the characteristic droplet or particle size and the resulting morphology of ice accretion, [13].

In the present study, the combined influence of the above-mentioned factors is described through the LWC, which represents the equivalent mass concentration of water (or water equivalent of snow) per unit volume of air. A combined LWC parameterization is employed to account for different physical mechanisms of icing.

For in-cloud icing associated with fog and ice fog, LWC is treated as a primary parameter and is prescribed based on typical values for high-latitude conditions, with additional dependence on air temperature and relative humidity, [14]. In cases of icing caused by supercooled liquid precipitation, the equivalent liquid water content is reconstructed from the precipitation intensity R using the empirical relationship given by equation (1), [14]:

$$w = 0.26R^{0.88} \tag{1}$$

Precipitation in the form of wet snow and rain–snow mixtures, whose adhesion mechanism differs from classical in-cloud icing, is also represented in the engineering model through an equivalent liquid water content. In this case, the equivalent mass concentration of water in air is estimated from the snowfall intensity using a mass-flux approximation:

$$w_{snow} = \frac{\rho_{snow}}{V_f}\frac{R}{3600} \tag{2}$$

In equation (2) ρ_{snow} is the density of wet snow, and V_f is the characteristic fall velocity of snow particles, taken to be approximately 1 m/s.

The equivalent liquid water content w_{snow} is applied only under wet-snow conditions, which occur within a narrow temperature range close to 0 °C at elevated relative humidity. This corresponds to the criterion of positive wet-bulb temperature ($t_w > 0$) proposed in [15]. Such a parameterization allows the icing rate to be directly linked to routinely observed meteorological variables obtained from standard weather station data and present weather codes (WW) according to the WMO classification, without explicit modeling of cloud and precipitation microphysics.

2.3 Kola WPP Conditions, Input Data, and Problem Statement

The Kola wind power plant is located in the northern part of the European territory of Russia and operates in a coastal zone characterized by prolonged periods of sub-zero air temperatures, high relative humidity, and frequent fog and snowfall events. These conditions promote both impingement-type and deposition-type icing of wind turbine blades, which may lead to power reduction, unstable rotor operation, and forced turbine shutdowns, [16].

To describe the meteorological conditions, archival data from the Teriberka weather station, located in the immediate vicinity of the Kola WPP site, were used. The following parameters were considered as input: air temperature, wind speed, relative humidity, atmospheric pressure, present weather type (WW code according to the WMO classification), and estimates of cloud base height. This set of variables allows characterization of both the thermodynamic state of the near-surface atmospheric layer and the type of precipitation and the presence of a supercooled liquid water phase.

As an additional characterization of the site climate, an analysis of the annual meteorological dataset was performed to estimate the total duration of periods potentially hazardous with respect to wind turbine blade icing. Such periods include episodes of wet snow, mixed precipitation (rain with snow) occurring at negative air temperatures, as well as fog events under sub-zero temperature conditions.

A summary of the cumulative duration of these meteorological conditions based on data from the Teriberka weather station is presented in Table 1.

Table 1. Duration of periods potentially hazardous for wind turbine blade icing

Type of condition	Total duration, h
Wet snow	≈350
Rain with snow	≈140
Cold fog	≈12

Source: created by the authors

The obtained estimates confirm that during the cold season, conditions favourable for ice accretion occur regularly and cumulatively occupy a significant fraction of time, which justifies the necessity of explicitly accounting for icing processes when modelling the operation of the Kola WPP.

Accurate determination of wind speed at hub height is of key importance for calculating wind turbine operating regimes. Therefore, wind speed V_2 at the hub height $h_2 = 84$ m was extrapolated from the measured wind speed V_1 at the anemometer height $h_1 = 10$ m using a power-law wind profile with exponent m, defined by equation (3)

$$V_2 = V_1 \left(\frac{h_2}{h_1}\right)^m \quad (3)$$

An analysis of wind speed observations from the Murmansk television tower within the surface layer of 24–140 m showed that the exponent m can vary over a relatively wide range (Figure 1).

Calculations performed using data from more than 20 meteorological stations made it possible to establish a relationship between the average value of m and the mean annual wind speed. This dependence is well approximated by the empirical equation (4), [17]:

$$\mathrm{m} = 0{,}60(V_1)^{-0{,}77} \quad (4)$$

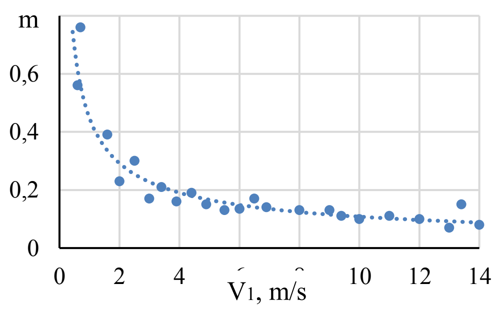

Fig. 1: Dependence of the power-law exponent m on wind speed at the anemometer height
Source: created by the authors

For the remaining meteorological parameters – air temperature, relative humidity, WW code, and the derived LWC – vertical homogeneity within the surface layer was assumed in the calculations. The values measured at the weather station were directly used to represent conditions at hub height.

An analysis of the annual time series of cloud base height showed that the minimum recorded cloud base height was approximately 50 m and occurred only during four three-hour intervals over the year. In the vast majority of cases, the cloud base was either absent or located well above 84 m. This indicates that episodes in which the wind turbine rotor was directly immersed in a low-level cloud layer were rare during the considered period.

Figure 2 shows the mean monthly air temperature and wind speed based on Teriberka weather station data, illustrating the pronounced seasonality of climatic conditions in the Kola WPP area.

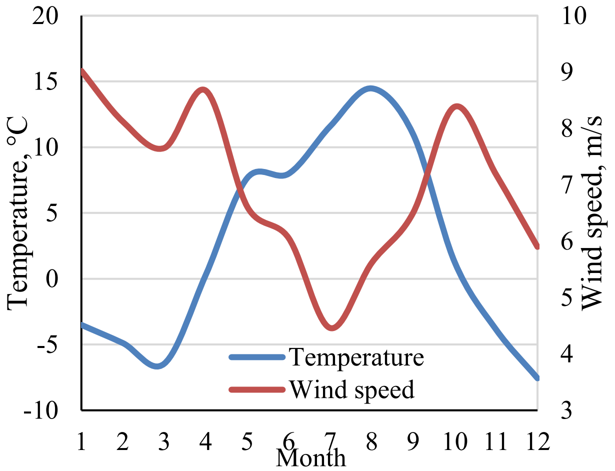

Fig. 2: Monthly meteorological characteristics in the Kola WPP area

Source: created by the authors

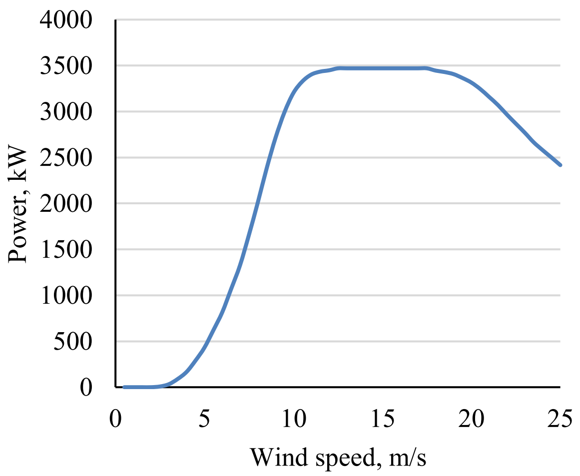

Fig. 3: Power curve of SG 3.4-132

Source: [17]

The Kola WPP consists of 57 Siemens Gamesa SG 3.4-132 wind turbines. The main technical characteristics of the turbine model are presented in Table 2, and the manufacturer's power curve is shown in Figure 3, [17]. In subsequent calculations, each individual wind turbine is assumed to be identical in terms of aerodynamic and energy performance, and the total wind farm energy production is obtained as the sum of the outputs of all 57 turbines.

Table 2. Technical data of SG 3.4-132

Rated power, kW	Hub height, m	Rotor diameter, m	Blade length, m
3465	84	132	64.5

Source: [17]

The problem formulation is as follows: given a time series of meteorological parameters and wind turbine characteristics, it is required to

– calculate the temporal evolution of ice mass and ice thickness on wind turbine blades using the Makkonen formulation;

– account for possible ice shedding and partial ice removal under changing meteorological conditions and turbine operating regimes;

– Assess the impact of icing on rotor rotational speed, possible turbine shutdowns, and the resulting losses in the integral energy production of the Kola wind power plant.

3 Methodology and Numerical Experiments

3.1 Input Data and Study Object

To develop and validate the icing model, archival meteorological data from the Teriberka weather station for a representative cold period were used. The dataset includes the following variables with a time step of $\Delta t = 3$ h:

– air temperature, T_a (°C);

– relative humidity, U (%);

– atmospheric pressure, p (Pa);

– mean wind speed at the meteorological measurement height, V_1 (m/s);

– precipitation rate, R (mm/h);

– present weather code, WW, according to the WMO classification (precipitation type and weather phenomena).

Based on these inputs, the liquid water content in the air was estimated, and the thermodynamic quantities required for the icing intensity coefficient in the Makkonen formulation were calculated. The assumptions regarding the vertical uniformity of thermodynamic variables and the extrapolation of wind speed to hub height are described in Section 2.3.

The modelling object at the level of an individual machine is a Siemens Gamesa SG 3.4-132 wind turbine, representative of the Kola WPP. The turbine power output as a function of wind speed is calculated using the manufacturer's power curve (Figure 3). Thus, the present work estimates the potential energy yield determined by meteorological conditions and turbine characteristics. External factors not directly related to aerodynamics – such as dispatch limitations, curtailment due to grid constraints, network restrictions, and planned or unplanned outages – are not considered.
Spatial variability of meteorological conditions within the wind farm area is neglected; it is assumed that all turbines experience identical ambient conditions at each time step.

In the model, each rotor blade is discretized along the span into 64 radial segments indexed by i = 1…64. For each segment, the mean radius r_i, chord length c_i, equivalent diameter D_i (characterising the effective flow-capture width in a cylindrical approximation), and effective moisture-capture area A_i are specified. This discretization enables the spanwise variation of blade geometry to be accounted for, along with the associated non-uniform distribution of ice mass and thickness. For each segment, the local relative flow velocity, LWC, and ice accretion rate are calculated; the segment-wise results are then aggregated to assess the impact of icing on rotor aerodynamic performance and electrical energy production.

Table 3. Empirical parameters used in the icing model (baseline values)

Variable/Parameter	Value
Liquid water content for in-cloud icing, w [18]	0,4 g/m^3
Median volume diameter in fog, MVD [18]	25 µm
Runback fraction, λ [19]	0,26
Recovery coefficient, r [19]	0,79
Saturated water vapour pressure at the ice surface, e_s [19]	617 Pa
Linearised radiation constant, a [19]	8,1x107 K^3
Ice adhesion strength, τ_{adm} [20]	200 kPa
Drag coefficient of an iced segment, Cd [21]	1,2
Lower threshold of relative ice thickness, Θ_{min} [22]	1%
Upper threshold of relative ice thickness, Θ_{max}[22]	5%

Source: created by the authors

In addition to the meteorological inputs and blade geometric characteristics, the model employs a set of empirical parameters describing ice accretion, surface heat-balance terms, mechanical ice shedding, and aerodynamic performance degradation. The nominal values used in the baseline scenario are provided in Table 3. The variation ranges of these parameters and their influence on the modelling results are analysed separately in Section 3.7.

3.2 Ice Mass Balance

To describe the dynamics of ice accretion on wind turbine blades, a balance scheme is introduced, in which the actual ice mass on a blade at time (t) is written as:

$$M_{res}(t) = M_{acc}(t) - M_{loss}(t) \qquad (5)$$

In equation (5) $M_{res}(t)$ is the total mass of ice accumulated due to atmospheric icing, and $M_{loss}(t)$ is the ice mass removed by melting, sublimation and mechanical shedding. The residual mass $M_{res}(t)$ is subsequently used to assess the impact of icing on rotor rotational speed and wind turbine power output. The accumulated ice mass is represented as a sum over radial blade segments, as shown equation (6):

$$M_{res}(t) = \sum_{i=1}^{N} m_i(t) \qquad (6)$$

where $m_i(t)$ is the ice mass on the (i)-th segment. Similarly, the ice mass loss can be decomposed into three components:

$$M_{loss}(t) = M_{melt}(t) + M_{sub}(t) + M_{shed}(t) \qquad (7)$$

In equation (7) $M_{melt}(t)$ is the ice mass removed by melting, $M_{sub}(t)$ is the mass lost due to sublimation, and $M_{shed}(t)$ is the mass of ice removed as a result of mechanical shedding (detachment) from the blade surface.

3.3 Icing Model

The rate of ice mass accretion on a given blade segment is described in formulation (8), [23]:

$$\frac{dm_i}{dt} = a_{1,i} \cdot a_{2,i} \cdot a_{3,i} \cdot w \cdot V_{rel,i} \cdot A_i \qquad (8)$$

where w is the liquid water content in air (LWC), $V_{rel,i}$ is the relative particle velocity, and A_i is the effective moisture-capture area of segment i. The coefficients $a_{1,i}$, $a_{2,i}$ and $a_{3,i}$ represent the collision efficiency, the collection (sticking) efficiency, and the freezing efficiency, respectively.

The collision efficiency a_1 is governed by the balance between inertial and aerodynamic forces acting on particles in the incoming flow. According to ISO 12494-2017, for precipitation icing (rain and wet snow) the collision efficiency for objects whose characteristic size is small relative to the droplet size is close to unity. Therefore, in the present study, a_1 is adopted for precipitation icing. For in-cloud icing associated with small supercooled droplets (fog and freezing fog), a_1 is calculated using Makkonen's empirical parameterization for a cylindrical collector, expressed via relevant dimensionless groups that include droplet diameter, the equivalent diameter of the blade segment, and air viscosity and density.

The collection efficiency a_2 describes the fraction of deposited moisture that remains on the surface after impact. For supercooled liquid droplets typical of fog, drizzle, and rain, $a_2 \approx 1$ is assumed, which corresponds to rapid freezing of the droplet and/or spreading over an existing liquid film. For dry snow, a_2 is assumed to be close to zero due to effective particle rebound. For wet snow and mixed precipitation, the collection efficiency is empirical and is non-zero only when the wet-snow criterion proposed by Makkonen is satisfied, i.e., when the wet-bulb temperature is positive ($t_w > 0$). In this work, a simplified temperature-based parameterization of a_2 is used to provide a smooth transition between negligible sticking at positive air temperatures and near-complete sticking under persistently sub-zero conditions.

The freezing efficiency a_3 represents the fraction of deposited water that actually transitions into the solid phase and is determined from the heat balance at the "flow–surface–environment" interface following the approach of [24]. The model accounts for convective and radiative heat exchange, latent heat effects associated with phase change, and possible runback of unfrozen water under wet icing conditions. A number of parameters entering the heat-balance expressions are empirical and are summarized in Table 3.

3.4 Ice Mass Loss Model

The loss of ice mass is treated as the sum of contributions from three processes: melting, sublimation and mechanical shedding. For each segment and time step, the corresponding mass changes are calculated, after which the residual ice mass is updated using equation (8).

3.4.1 Ice melting

Ice melting is modelled on the basis of a steady-state heat balance in the near‑ surface layer, which includes convective heat exchange with the air, incoming shortwave solar radiation, longwave exchange with the sky, and heat input from liquid precipitation, [25]. For the (i)-th blade segment, the resulting surface heat flux at the ice–air interface is written in the form of equation (9):

$$q_{net,i} = q_{conv,i} + q_{SW,i} + q_{LW,i} + q_{rain,i} \qquad (9)$$

where $q_{conv,i} = h_i(T_a - T_s)$ is the convective heat flux, and $q_{SW,i}$, $q_{LW,i}$, $q_{rain,i}$ are the contributions of shortwave radiation, longwave radiation and liquid precipitation, respectively.

When $q_{net,i} > 0$, the incoming heat flux is used to melt the ice. The melting rate per unit area for the (i)-th segment is given by equation (10)

$$\dot{m}_{melt,i} = \frac{q_{net,i}}{L_f} \qquad (10)$$

and the ice mass melted on the segment over a time step Δt is calculated using equation (11)

$$\mathbf{\Delta} \boldsymbol{m}_{melt,i} = \dot{m}_{melt,i} A_i \Delta t \qquad (11)$$

The total ice mass removed by melting on the blade is obtained by summing the segment-wise contributions, as shown in equation (12):

$$M_{melt}(t + \Delta t) = M_{melt}(t) + \sum_{i=1}^{N} \mathbf{\Delta} \boldsymbol{m}_{melt,i} \qquad (12)$$

The implementation of the heat balance in the numerical model accounts for the site's geographic coordinates, the diurnal and annual variation of solar elevation, total cloud cover and the current weather code WW. However, in the present work these calculations are presented in a simplified, aggregated form.

3.4.2 Ice Sublimation

Ice sublimation is treated as diffusive mass transfer of water vapour between the ice surface and the surrounding air. For the (i)-th segment, the sublimation mass flux per unit area is given by equation (13), [26]:

$$\dot{m}_{sub,i} = h_{m,i} \left(\rho_{v,s} - \rho_{v,\infty} \right) \qquad (13)$$

where $h_{m,i}$ is the mass transfer coefficient, determined by analogy with convective heat transfer through the Schmidt number Sc (equation 14) and the Sherwood number Sh_i for cylindrical bodies (equation 15), [27]:

$$h_{m,i} = \frac{Sh_i D_v}{L_{c,i}} \qquad (14)$$

$$Sh_i = 0{,}61 Re_i^{\frac{1}{2}} Sc^{\frac{1}{3}} \qquad (15)$$

D_v is the diffusion coefficient of water vapour in air, and $p_{v,s}$ and $p_{v,\infty}$ are the water vapour densities at the ice surface and in the free stream, respectively.

The ice mass lost due to sublimation on the segment over a time interval Δt is calculated using equation (16)

$$\boldsymbol{\Delta m_{sub,i}} = \max\left(0, \dot{m}_{sub,i}\right) A_i \boldsymbol{\Delta}\mathrm{t} \quad (16)$$

where, in the numerical implementation, sublimation is taken into account only when the air is not saturated with respect to water vapour and the ice surface temperature is below 0 °C. The total ice mass loss due to sublimation on the blade is obtained by summation over all segments according to equation (17):

$$M_{sub}(t + \boldsymbol{\Delta}\mathrm{t}) = M_{sub}(t) + \sum_{i=1}^{N} \boldsymbol{\Delta m_{sub,i}} \quad (17)$$

3.4.3 Mechanical Shedding of Ice

Mechanical shedding (detachment) of ice from wind turbine blades is described by comparing the mechanical stresses in the ice layer with the limiting adhesive strength of the ice–surface interface. For the (i)-th segment, the following forces are considered, [26]:

– The centrifugal force is defined by equation (18):

$$F_{c,i} = m_{ice,i} \omega^2 r_i \quad (18)$$

where $m_{ice,i}$ is the ice mass on the segment, ω is the rotor angular speed, and r_i is the segment radius;

– The aerodynamic drag force is given by equation (19):

$$F_{d,i} = \frac{1}{2} \rho_a \boldsymbol{V_{rel,i}^2 C_d A_i} \quad (\mathbf{19})$$

where $\boldsymbol{C_d}$ is the drag coefficient of the iced segment;

– The ice weight is calculated using equation (20):

$$F_{g,i} = m_{ice,i} g \quad (20)$$

which, under the considered conditions, generally plays a secondary role compared with centrifugal and aerodynamic loads.

The resulting forces are converted into normal and shear stresses at the ice–surface interface using equations (21) and (22), [28]:

$$\sigma_{n,i} \approx \frac{\boldsymbol{F_{c,i} + F_{d,i}}}{\boldsymbol{A_i}} \quad (\mathbf{21})$$

$$\tau_{s,i} \approx \frac{\boldsymbol{F_{d,i}}}{\boldsymbol{A_i}} \quad (\mathbf{22})$$

To assess ice shedding, an equivalent stress combining the normal and shear stress components is introduced. This equivalent stress is defined by equation (23):

$$\tau_{eq,i} = \sqrt{\tau_{s,i}^2 + \sigma_{n,i}^2} \quad (\mathbf{23})$$

Ice shedding on a segment is assumed to occur when the equivalent stress $\tau_{eq,i}$ exceeds a threshold value τ_{adm}, interpreted as the effective adhesive strength of the ice–surface interface. The ice mass removed during one time step is then determined by the threshold rule given in equation (24):

$$\boldsymbol{\Delta m_{shed,i}} = \begin{cases} m_{ice,i}, & \tau_{eq,i} \geq \tau_{adm} \\ \mathbf{0}, & \tau_{eq,i} < \tau_{adm} \end{cases} \quad (24)$$

Such an approach reflects the threshold character of adhesive failure and allows avoiding the introduction of additional empirical functions, whose parameterization would require experimental or high-fidelity numerical data.

The total ice mass removed due to mechanical shedding is obtained by summation over segments, as expressed in equation (25):

$$M_{shed}(t + \boldsymbol{\Delta}\mathrm{t}) = M_{shed}(t) + \sum_{i=1}^{N} \boldsymbol{\Delta m_{shed,i}} \quad (25)$$

The described approach represents an engineering extension of the classical Makkonen model, in which ice fracture and shedding processes are not explicitly considered. In the present work, mechanical shedding is modelled through a comparison of averaged mechanical stresses with the effective adhesive strength of the ice–surface interface, without resolving the detailed micromechanics of ice failure. The adopted criterion assumes uniform stress distribution over the contact area of each blade segment. The values of the drag coefficient and adhesive strength were taken within ranges characteristic of different types of atmospheric icing and cold coastal climates, based on literature data.

3.5 Model of the Impact of Residual Ice on Rotor Aerodynamics and Wind Turbine Power

The relationship between the calculated residual ice mass $M_{ice}(t)$ and the electrical power output of a wind turbine is implemented in this study through a simplified engineering model of rotor aerodynamic degradation. The model is based on the assumption that the accumulation of ice on the blades increases the effective airfoil thickness and surface roughness [22], which leads to a reduction in lift and an increase in drag. As a consequence, the rotor power coefficient and rotational speed decrease.

For each radial blade segment, the equivalent ice layer thickness is determined from the calculated ice mass $m_{ice,i}$ and effective area A_i using equation (26):

$$\delta_i(t) = \frac{m_{ice,i}(t)}{\rho_{ice} A_i} \quad (26)$$

where ρ_{ice} is the ice density. To account for the influence of ice on local aerodynamic characteristics, the relative ice thickness is introduced as:

$$\Theta_i(t) = \frac{\delta_i(t)}{c_i} \quad (27)$$

In equation (27) c_i is the chord length of the (i)-th segment. It is assumed that for small values of Θ_i the presence of ice has a negligible effect on airfoil aerodynamics, whereas an increase of Θ_i to several percent of the chord leads to a pronounced degradation of blade performance.

To quantify this effect, a dimensionless local coefficient of preserved aerodynamic efficiency $f_i\Theta_i$ (ranging from 0 to 1) is introduced, interpreted as the relative retention of the "ideal" aerodynamic characteristics (lift, power coefficient, etc.) on the given segment:

$$f_i\Theta_i = \begin{cases} 1, & \Theta_i \le \Theta_{min} \\ 1 - \dfrac{\Theta_i - \Theta_{min}}{\Theta_{max} - \Theta_{min}}(1 - \mathrm{f_{min}}), & \Theta_{min} < \Theta_i < \Theta_{max}, \\ \mathrm{f_{min}}, & \Theta_i < \Theta_{max} \end{cases} \quad (28)$$

In equation (28), indicative threshold values adopted from Table 3 are used: $\Theta_{min} = 0.01$, $\Theta_{max} = 0.05$, with a minimum retained efficiency $\mathrm{f_{min}} = 0.2$. Thus, for a relative ice thickness below 1 % of the chord, its influence is considered negligible ($\mathrm{f}_i \approx 1$), whereas for $\Theta_i \ge$ 5%) the corresponding blade section is treated as strongly degraded in aerodynamic performance. The values of f_i are further constrained to the interval ([0, 1]), which prevents non-physical results in borderline regimes.

Taking into account that the contribution of individual radial blade segments to the rotor torque and power is non-uniform and increases towards the blade tip, the rotor-averaged coefficient of preserved aerodynamic efficiency $F_{avg}(t)$ is calculated as a radius-weighted average using equation (29):

$$F_{avg}(t) = \frac{\sum_{i \epsilon I(t)} W_i f_i\left(\Theta_i(t)\right)}{\sum_{i \epsilon I(t)} W_i}, \quad (29)$$

The weighting factor W_i used in equation (29) is defined by equation (30):

$$W_i = r_i^3 \quad (30)$$

where $I(t)$ is the set of blade segments for which the geometry is well defined, and ice may be present.

The choice of the weighting factor $W_i = r_i^3$ is motivated by the fact that, for an axially symmetric rotor, the local contribution of a radial annulus to the torque and power scales as r_i^3. Consequently, icing closer to the blade tips has a substantially stronger impact on energy production than ice accretion near the blade root. The weighted averaging allows this sensitivity distribution to be accounted for without explicitly solving the blade aerodynamic problem. The coefficient $F_{avg}(t)$ is interpreted as an integral measure of rotor aerodynamic degradation under icing conditions.

Within the framework of this study, it is assumed that the rotor rotational speed in icing conditions scales proportionally to the rotor-averaged coefficient of preserved aerodynamic efficiency. This assumption is expressed by equation (31):

$$n_{ice} = n_{no,ice}(t) * F_{avg}(t) \quad (31)$$

where $n_{no,ice}(t)$ is the calculated (or rated) rotational speed of the turbine in the absence of ice for the given wind speed and control regime. Thus, when $F_{avg}(t) \approx \mathbf{1}$, the rotor operates almost in an "ice-free" regime, whereas a decrease of $F_{avg}(t)$ to 0.3–0.4 leads to a substantial reduction in rotational speed and, consequently, in power output.

Additionally, a threshold shutdown criterion is introduced for severe icing conditions. This criterion is formulated as the inequality in equation (32):

$$F_{avg}(t) < F_{stop} \quad (32)$$

where F_{stop} is a threshold value (in the calculations, F_{stop} = 0.3), it is assumed that the turbine is stopped for safety reasons and/or by the control system algorithms, and its electrical power at that time is set to zero. In the subsequent calculation of the Kola WPP production (Section 3.6), the power of an individual turbine in each hourly interval is determined based on the wind speed at hub height, the adjusted rotational speed, and the manufacturer's power curve, accounting for possible shutdowns.

3.6 Simulation Results with Icing Taken into Account

Using the described icing model, simulations of the Kola wind power plant (WPP) energy production for 2023 were performed in two operating modes:

1. without accounting for blade icing (conditionally "clean" blades);
2. with ice accumulation and partial removal, calculated using the Makkonen formulation.

For each 3-hour time interval, the measured wind speed at the meteorological sensor height was extrapolated to the hub height, after which the instantaneous power output of an individual wind turbine was determined from the Siemens Gamesa SG 3.4-132 power curve.

It should be emphasized that the energy production calculated in the present study represents potential aerodynamically driven power output and is not intended for direct comparison with the actual electricity generation of the Kola WPP, which is strongly affected by dispatch constraints, grid-related curtailment, and operational downtime, [29].

The total wind farm power was obtained as the product of the power output of a single turbine and the total number of turbines (57 units). Due to the lack of spatially distributed meteorological observations across the site, it was assumed that all turbines are exposed to identical external conditions and experience the same degree of icing at any given time.

In the icing scenario, the calculated power output was additionally corrected to account for the degradation of rotor aerodynamic performance caused by ice accretion, as well as for possible turbine shutdowns when critical icing thresholds were reached.

Figure 4 presents the annual energy production profiles of the Kola WPP for the scenarios with and without icing. A pronounced impact of icing is observed during the cold period of the year (January–April and October–December), when the simulated energy production in the icing scenario is systematically lower than that in the "clean" case. This behavior corresponds to the increased recurrence of adverse meteorological conditions during these months.

Monthly aggregation of the results (Figure 4) shows that the relative energy production losses due to icing vary approximately between 2 % and 15 %, depending on the month. The largest losses are obtained for March and December, which are associated with the combination of elevated wind speeds and air temperatures close to 0 °C. These transitional periods are characterized by frequent occurrences of wet snow and supercooled liquid precipitation, which, according to the analysis of meteorological data, constitute the dominant icing mechanisms for the Kola WPP. In colder winter months, when the liquid water content in the air is lower, the intensity of precipitation-related and mixed icing decreases, resulting in smaller relative production losses compared with transitional periods.

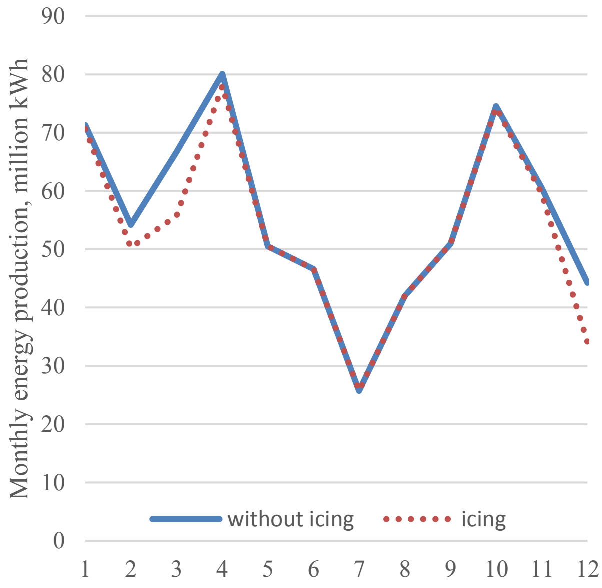

Fig. 4: Annual energy production profiles with and without icing

Source: created by the authors

The integral annual energy production of the Kola WPP in the simulations without and with icing amounted to 667 and 638 million kWh, respectively. Comparison of these values indicates that the total energy production losses associated with blade icing in 2023 are on the order of 5 % of the potential annual wind farm output in the absence of ice. This estimate should be interpreted as a model-based assessment under the adopted assumptions; nevertheless, it is consistent in order of magnitude with the results of international studies for wind farms operating in similar cold and humid high-latitude environments, where precipitation-induced icing plays a dominant role, [30].

3.7 Sensitivity Analysis

The sensitivity analysis focused on the parameters that have the strongest impact on rotor aerodynamic degradation and wind turbine operating regimes.

These include the lower and upper thresholds of relative ice thickness, Θ_{min} and Θ_{ax}, used in the aerodynamic degradation function, as well as the ice adhesive strength τ_{adm} employed in the mechanical shedding criterion. Parameters related exclusively to in-cloud (fog-induced) icing, such as the characteristic droplet size, were not analyzed separately, since the total duration of such conditions during the considered year was small (approximately 12 h) compared to the duration of precipitation-induced and mixed icing events.

The sensitivity analysis was performed by varying one parameter at a time within physically reasonable ranges while keeping all other parameters fixed, followed by recalculation of the annual energy production for 2023. The results of the analysis are summarized in Table 4, which reports both the annual energy production in the icing scenario and the corresponding relative production losses with respect to the ice-free case.

Table 4. Sensitivity analysis of annual energy production losses with respect to key empirical model parameters

Parameter	Variation range	Energy production, million kWh	Losses, %
Θ_{min}	0,05-0,15	635-642	3,7-4,8
Θ_{max}	0,4-0,6	636-640	4,0-4,6
τ_{adm}	150-300	638	4,3

Source: created by the authors.

As follows from Table 4, variation of the aerodynamic degradation thresholds Θ_{min} and Θ_{max} within physically justified limits leads to changes in the integral annual loss estimate on the order of approximately one percentage point, while preserving the overall order of magnitude of the losses. This indicates that the conclusions regarding the impact of icing on the annual energy production of the Kola WPP are robust with respect to reasonable variations of these parameters.

Within the adopted modelling framework, variation of the adhesive strength τ_{adm} does not produce a noticeable effect on the calculated annual energy production. This is explained by the fact that, for wind turbines without dedicated anti-icing or de-icing systems, the effective adhesive strength of ice is typically higher than the mechanical stresses acting on the ice layer under characteristic operating conditions, as reported in the literature. As a result, the mechanical ice shedding mechanism is not activated in the simulations and does not constitute a dominant factor in energy production losses, which are primarily governed by aerodynamic performance degradation and turbine shutdown regimes.

Thus, the numerical experiment confirms that blade icing represents a significant factor limiting the realizable energy potential of the Kola WPP and should be explicitly taken into account when assessing expected energy production, planning operational strategies, and evaluating potential icing mitigation measures.

4 Conclusion

The present study was aimed at a quantitative assessment of the potential impact of atmospheric blade icing on the energy production of the Kola wind power plant (WPP) and at the development of an engineering-level modelling approach suitable for application under conditions of limited meteorological information. Based on archival data from the Teriberka weather station and on the technical characteristics of Siemens Gamesa SG 3.4-132 wind turbines, a numerical icing model was developed using the Makkonen formulation with a parameterization of LWC derived from air temperature, relative humidity, and the present weather code. Icing processes were simulated on discretized blade segments with account taken of local geometry and relative flow velocity, which enabled the linkage between spanwise ice accretion, aerodynamic performance degradation, and changes in turbine power output.

The simulation results indicate that, under the climatic conditions of the Kola WPP, blade icing exhibits a pronounced seasonal character and is most significant during the cold period of the year (January–April and October–December). The largest relative production losses were obtained for March and December, which are associated with the frequent occurrence of wet snow and supercooled precipitation at air temperatures close to 0 °C. In individual months of the cold season, relative energy production losses reach approximately 15 %, whereas during the warm period, the impact of icing on wind farm operation is negligible. The integral estimate for 2023 indicates a reduction of annual energy production by about 4–5 % compared with the ice-free scenario. This value should be interpreted as a model-based estimate under the adopted assumptions; nevertheless, it is consistent in order of magnitude with results reported in international studies for wind farms operating in similar cold and humid high-latitude environments dominated by precipitation-induced icing.

The sensitivity analysis confirmed the robustness of the obtained results with respect to reasonable variations of key empirical model parameters and demonstrated that, within the adopted framework, the dominant contribution to production losses arises from aerodynamic performance degradation and turbine shutdown regimes, while mechanical ice shedding does not play a governing role.

The proposed model is intended for preliminary engineering assessment of icing impacts in northern regions, for the analysis of operating regimes, and for substantiating the need for anti-icing or de-icing measures. At the same time, the results should not be interpreted as a direct validation against actual operational losses, due to simplifying assumptions such as the use of data from a single meteorological station, simplified LWC parameterization, and the absence of explicit modelling of spatial variability and detailed rotor aerodynamics. Future work should focus on refining the LWC parameterization and model coefficients based on dedicated measurements, incorporating spatially and vertically resolved meteorological data (e.g., NWP and SCADA), and comparing model predictions with observed operational data from the Kola WPP.

References:

[1] A. M. Bramm, S. A. Eroshenko, Evaluation of the impact of the distance determination function on the results of optimization of the geographical placement of renewable energy sources-based generation using a metaheuristic algorithm, *Journal of Mining Institute*, Vol. 271, 2025, pp. 141–153, [Online]. https://pmi.spmi.ru/pmi/article/view/16333 (Accessed Date: March 2, 2026).

[2] D. A. Ustinov, E. R. Shafhatov, Assessment of reliability indicators of combined systems of offshore wind turbines and wave energy converters, *Energies*, Vol. 15, 2022. DOI: 10.3390/en15249630.

[3] O. Fakorde, Z. Feger, H. Ibrahim, A. Ilinca, J. Perron, C. Masson, Ice protection systems for wind turbines in cold climate: characteristics, comparisons and analysis, *Renewable and Sustainable Energy Reviews*, Vol. 65, 2016, pp. 662–675. DOI: 10.1016/j.rser.2016.06.080.

[4] L. T. Contreras, S. Lain, A. Ilinca, A review on the estimation of power loss due to icing in wind turbines, *Energies*, Vol. 15, 2022. DOI: 10.3390/en15031083

[5] Y. Zhukovskiy, A. Stoianova, P. Tsvetkov, A. Buldysko, Scenario modeling of sustainable development of energy supply in the Arctic, *Resources*, Vol. 10, No. 124, 2021. DOI: 10.3390/resources10120124

[6] V. A. Shpenst, A. A. Belsky, E. A. Orel, Improving the efficiency of autonomous electrical complexes with renewable energy sources by adaptive regulation of operating modes, *Journal of Mining Institute*, Vol. 261, 2023, pp. 479–492, [Online]. https://pmi.spmi.ru/pmi/article/view/16177 (Accessed Date: May 2, 2026)

[7] Z. Chuang, H. Yi, X. Chang, H. Liu, H. Zhang, L. Xia, Comprehensive analysis of the impact of icing of wind turbine blades on power loss in cold regions, *Journal of Marine Science and Engineering*, Vol. 11, 2023. DOI: 10.3390/jmse11061125.

[8] N. G. Lyubimova, A. S. Flaxman, A. G. Redin, A. D. Kuchkina, Potential and development prospects of wind generation on the Kola Peninsula, *Vestnik Universiteta*, No. 5, 2024, pp. 116–128. DOI: 10.26425/1816-4277-2024-5-116-128.

[9] X. Yang, X. Bai, H. Cao, Influence analysis of rime icing on aerodynamic performance and output power of offshore floating wind turbines, *Ocean Engineering*, Vol. 258, 2022. DOI: 10.1016/j.oceaneng.2022.111725.

[10] A. G. Kraj, E. L. Bibeau, Phases of icing on wind turbine blades characterized by ice accumulation, *Renewable Energy*, Vol. 35, 2010, pp. 966–972. DOI: 10.1016/j.renene.2009.09.013.

[11] F. Lamraoui, G. Fortin, R. Benoit, J. Perron, C. Masson, Atmospheric icing impact on wind turbine production, *Cold Regions Science and Technology*, Vol. 100, 2014, pp. 36–49. DOI: 10.1016/j.coldregions.2013.12.008.

[12] Z. Zhang, H. Zhang, X. Zhang, Q. Hu, X. Jiang, A review of wind turbine icing and anti-/de-icing technologies, *Energies*, Vol. 17, 2024. DOI: 10.3390/en17122805..

[13] Z. Xu, T. Zhang, X. Li, Y. Li, Effects of ambient temperature and wind speed on icing characteristics and anti-icing energy demand of a blade airfoil for wind turbines, *Renewable Energy*, Vol. 217, 2023. DOI: 10.1016/j.renene.2023.119135.

[14] E. Sundin, L. Makkonen, Estimation of ice loads on a lattice tower by weather station data, *Journal of Applied Meteorology*, Vol. 37, No. 5, 1998, pp. 523–529. DOI: 10.1175/1520-0450(1998)037<0523:ILOALT>2.0.CO;2.

[15] L. Makkonen, Estimation of wet snow accretion on structures, *Cold Regions Science and Technology*, Vol. 17, 1988, pp. 83–88. DOI: 10.1016/S0165-232X(89)80018-7.

[16] L. Gao, Y. Liu, L. Ma, H. Hu, A hybrid strategy combining minimized leading-edge electric heating and superhydro-/ice-phobic surface coating for wind turbine icing mitigation, *Renewable Energy*, Vol. 140, 2019, pp. 943–956. DOI: 10.1016/j.renene.2019.03.112.

[17] V. F. Beley, G. V. Kotsar, Assessment of wind energy potential of the Murmansk Region and performance of the Kola wind farm (Оценка ветроэнергетического потенциала Мурманской области и эффективности Кольской ВЭС), *Vestnik of MSTU*, Vol. 23, No. 4, 2020, pp. 376–386. DOI: 10.21443/1560-9278-2020-23-4-376-386.

[18] P. Blasco, J. Palacios, S. Schmitz, Effect of icing roughness on wind turbine power production, *Wind Energy*, Vol. 20, No. 4, 2017, pp. 601-617. DOI: 10.1002/we.2026.

[19] International Organization for Standardization, ISO 12494:2017, *Atmospheric icing of structures*, International Organization for Standardization, Geneva, 2017, [Online]. https://www.iso.org/standard/72443.html (Accessed Date: March 2, 2026).

[20] K. Zietkowska, R. Kozera, B. Przybyszewski, A. Boczkowska, B. Sztorch, D. Pakuła, B. Marciniec, R. E. Przekop, Hydro- and icephobic properties and durability of epoxy gelcoat modified with double-functionalized polysiloxanes, *Materials*, Vol. 16, 2023, Article 875. DOI: 10.3390/ma16020875.

[21] P. Górski, M. Tatara, S. Pospíšil, S. Kuznetsov, Model investigations of the aerodynamic coefficients of iced cables in cable-stayed bridges, *Czasopismo Techniczne*, 2019. DOI: 10.4467/2353737XCT.19.083.10862.

[22] Bragg, M. B., Broeren, A. P., Stirling, L., Ice-airfoil aerodynamics, *Progress in Aerospace Sciences*, Vol. 41, 2005, pp. 323–362. DOI: 10.1016/j.paerosci.2005.07.001.

[23] L. Makkonen, J. Zhang, T. Karlsson, M. Tiihonen, Modelling the growth of large rime ice accretions, *Cold Regions Science and Technology*, Vol. 151, 2018, pp. 133–137. DOI: 10.1016/j.coldregions.2018.03.014.

[24] H. Dobesch, D. Nikolov, L. Makkonen, Physical processes, modelling and measuring of icing effects in Europe, *Österreichische Beiträge zu Meteorologie und Geophysik*, Vienna, Austria, 2005, 75 p., [Online]. https://opac.geologie.ac.at/ais312/dokumente/OEBMG_34.pdf (Accessed Date: May 2, 2026).

[25] W. Yang, T. Chen, Y. Teng, S. Wu, P. Sun, Natural ice-melting mechanism of wind turbine blades in hilly and mountainous wind farms, *Proceedings of the 9th International Conference on Power and Renewable Energy*, Guangzhou, China, 2024, pp. 716-722. DOI: 10.1109/ICPRE62586.2024.10768439.

[26] G. Fortin, J. Perron, Wind turbine icing and de-icing, *Proceedings of the 47th AIAA Aerospace Sciences Meeting*, Orlando, USA, 2009, pp. 2976–2999. DOI: 10.2514/6.2009-274.

[27] F. Montagnaro, Sherwood (Sh) number in chemical engineering applications — a brief review, *Energies*, Vol. 17, 2024. DOI: 10.3390/en17174342..

[28] H. Beaugendre, F. Morency, F. Gallizio, Simulation of ice shedding around an airfoil, *Proceedings of the AIAA Atmospheric and Space Environments Conference*, Toronto, ON, Canada, 2010, DOI: 10.2514/6.2010-7984.

[29] V. V. Elistratov, V. A. Antonov, Energy and economic analysis of the operation of the Arctic wind farm in the Kola power grid (Энергоэкономический анализ работы арктической ветроэлектростанции в Кольской энергосистеме), *SOK*, Vol. 9, 2025, pp. 76–79, [Online]. https://www.c-o-k.ru/articles/energoekonomicheskiy-analiz-raboty-arkticheskoy-vetroelektrostancii-v-kolskoy-energosisteme (Accessed Date: March 2, 2026).

[30] E. Andersen, E. Börjesson, P. Vainionpää, L. S. Undem, *Wind power in cold climate*, Final Report, WSP Environmental for Nordic Energy Research, Oslo, Norway. 2011. https://www.nordicenergy.org/app/uploads/2012/01/wind_power_in_cold_climate_-_final_report.pdf (Accessed Date: March 2, 2026).

Contribution of Individual Authors to the Creation of a Scientific Article (Ghostwriting Policy)

The authors equally contributed to the present research, at all stages from the formulation of the problem to the final findings and solution.

Sources of Funding for Research Presented in a Scientific Article or the Scientific Article Itself

No funding was received for conducting this study.

Conflict of Interest

The authors have no conflicts of interest to declare.